Journal of Molecular Graphics and Modelling 54 (2014) 54–61

Contents lists available at ScienceDirect

Journal of Molecular Graphics and Modelling

journal homepage: www.elsevier.com/locate/JMGM

Ab initio molecular simulations for proposing potent inhibitors to butyrylcholinesterases

Takeru Murakawa [a], Yuki Matsushita [a], Tomoya Suzuki [a], Mahmud Tareq Hassan Khan [b], Noriyuki Kurita [a,*]

[a] *Department of Computer Science and Engineering, Toyohashi University of Technology, Tempaku-cho, Aichi 441-8580, Japan*
[b] *Holmboevegen 3B, 9010 Tromsø, Norway*

ARTICLE INFO

Article history:
Accepted 4 September 2014
Available online 18 September 2014

Keywords:
Alzheimer's disease
Acetylcholinesterase
Butyrylcholinesterase
Inhibitors
Molecular simulation
Molecular docking
s

ABSTRACT

Butyrylcholinesterase (BChE) exists mainly at neuromuscular junctions and plays an important role in the hydrolyzing mechanism of neurotransmitter acetylcholine. A variety of compounds have been produced in order to inhibit the function of BChE. We here investigate the specific interactions between BChE and some ligands (Kx) with large binding affinity to BChE, using ligand-docking, classical molecular mechanics and *ab initio* fragment molecular orbital (FMO) methods. The binding energies between BChE and Kx evaluated by the FMO method have a correlation with the 50% inhibition concentration obtained by the previous experiments. In addition, the FMO calculations highlight that Asp70, Trp82 and Tyr128 residues of BChE contribute significantly to the binding between BChE and Kx. Based on the results, we propose some novel ligands and elucidate that one of the proposed ligands can bind strongly to BChE. The present results are useful for developing potent inhibitors to BChE.

1. Introduction

In the mechanism of signal processing in living organisms, a nerve cell determines appropriate actions corresponding to various signals and sends new signals to its adjacent nerve cells [1]. Some of the nerve cells send the signal directly to muscle cells, leading to a movement of muscles, which is an essential action for living organisms. Therefore, these signal transfers are indispensable for living organisms to response to the change in environment, and the signals should be transferred between the nerve and the muscle cells with swiftness and accuracy [2].

Neurotransmitter substances play an essential role in the transmission of nerve signals between cells [3]. These small substances are released from the nerve cells and diffuse rapidly into the adjacent nerve cells to control their functions properly. For example, acetylcholine (ACh) exists at a synapse between nerve and muscle cells and transmits the nerve signals from the nerve to the muscle cells [4]. In the signal transmitting process in motor nerve cells, ACh is released into a muscle cell through a synapse and reacts to the receptor of the muscle cell to make it open, leading to a muscle contraction. The reacted ACh should be hydrolyzed immediately, because the remained ACh can be recognized as a new signal to react in the muscle cell by mistake.

The hydrolyzing mechanism of ACh is controlled by cholinesterases (ChEs) [5]. They are divided into two groups: acetylcholinesterase (AChE) and butyrylcholinesterase (BChE). AChE hydrolyzes ACh faster than the other ChEs and exists mainly at neuromuscular junctions and synapses of cholinergic brains, while BChE has higher activity in liver, intestine, heart, kidney and lung. The previous experiment [6] elucidated that the Ser200 residue existing at the active site of AChE binds specifically to the acetyl group of ACh and hydrolyzes it into choline and acetyl hydroxide and that a water molecule breaks the bond between Ser200 and ACh in a few milliseconds. Accordingly, AChE is an indispensable enzyme for controlling the mechanism of signal transmission from the nerve to the muscle cells. On the other hand, BChE preferentially acts on butyrylcholine (BCh), although it also hydrolyzes ACh. Since BChE hydrolyzes ester-containing drugs and scavenges the inhibitors of ChE before they reach their synaptic targets, BChE is toxicologically important [7]. In the absence of AChE, hippocampal ACh levels are regulated by BChE activity. This is one of the important roles of BChE in brain; hydrolysis of ACh when AChE activity is inhibited.

Recently, AChE and BChE have attracted much attention because of the possibility that they may contribute to ACh hydrolysis in

* Corresponding author. Tel.: +81 532 44 6875; fax: +81 532 44 6875.
E-mail addresses: kurita@cs.tut.ac.jp, nkuri0303@yahoo.co.jp (N. Kurita).

http://dx.doi.org/10.1016/j.jmgm.2014.09.002
1093-3263/

the brain of Alzheimer's patients [8]. Since an adequate amount of ACh is contained in intact brains, the hydrolysis of some ACh causes no serious problem in living organisms. In contrast, the brain of a person diagnosed with Alzheimer's disease usually has a considerable shortage of ACh, so that the transmission mechanism of information between nerve cells is damaged. It is thus expected that if the hydrolysis reaction of ACh by AChE and BChE can be inhibited in the brain of Alzheimer's patients, the amount of ACh in the synapse will not be decreased so significantly and the transmission mechanism will become smoother. Many types of ligands have been produced for inhibiting the hydrolysis reaction by AChE [9–11].

In the previous study [12], we investigated the specific interactions between AChE and several carbamates Bx (x = 1–7) and proposed some potent inhibitors for AChE, using molecular simulations based on classical molecular mechanics (MM) and *ab initio* fragment molecular orbital (FMO) methods. The ligands Bx are mainly composed of glycine, benzene and dimethylaniline. We first confirmed the validity of the molecular simulations by the comparison between the results obtained by the simulations and the previous experiments [13]. Subsequently, some novel ligands were proposed based on the results simulated, and their specific interactions with AChE were investigated by the FMO calculations at an electronic level. From the results simulated, we proposed a novel ligand, which binds strongly to AChE, as a potent inhibitor for AChE. On the other hand, as for the inhibitor to BChE, there are only a few studies including the previous experimental study [14].

In the present study, we investigate the specific interactions between BChE and some types of ligands, whose properties were investigated by our previous experiments [9]. Based on the results evaluated, we proposed novel ligands, which have strong binding affinity to BChE. These ligands can be potent inhibitors for both AChE and BChE.

2. Details of molecular simulations

2.1. Structure optimization for solvated BChE + ligand complexes

In the previous experiment [9], the 50% inhibition concentration (IC_{50}) values of 26 types of ligands Kx (x = 1–26) were investigated for inhibiting the functions of AChE and BChE. The IC_{50} values are compared in Fig. S1 of the supporting materials. In the present study, we first employed four types of ligands (K01, K07, K16 and K25) among the Kx ligands, in order to elucidate which parts of these ligands contribute to the binding to BChE. K01 and K07 have the maximum and the minimum IC_{50} value for BChE, respectively, while K16 and K25 have the maximum and the minimum IC_{50} value for AChE. The chemical structure formulas of these ligands are shown in Fig. 1. Their initial structures were constructed by using molecular modeling program HyperChem 8.0.4, and they were optimized in vacuum by B3LYP/6-31G(d,p) method of Gaussian03 [15] in a similar way as the previous DFT study [16].

As an initial structure of BChE, we employed the X-ray crystal structure [17] registered in protein data bank PDB (PDB ID is 1P0P), because this structure has some crystal water molecules. This structure is consisted of 523 amino acids from the 4th to the 529th residues, and the information of the 378th, 379th and 455th residues is missing in the PDB file. These residues do not exist near the ligand-binding pocket of BChE. The protonation states for His residues of BChE were determined based on the pK_a values evaluated by the PROPKA Web Interface2.0 (http://propka.ki.ku.dk/). His residues with pK_a value larger than 6.0 were assigned as Hip, while the other His residues were assigned as Hid.

To obtain candidate structures for the BChE + Kx complex, we used the automated protein-ligand docking program Autodock 4.2 [18], because the same program was used for docking ligands to AChE in the previous study [19]. At first, we docked butyrylcholine (BCh) to BChE and compared the docked structure with the PDB

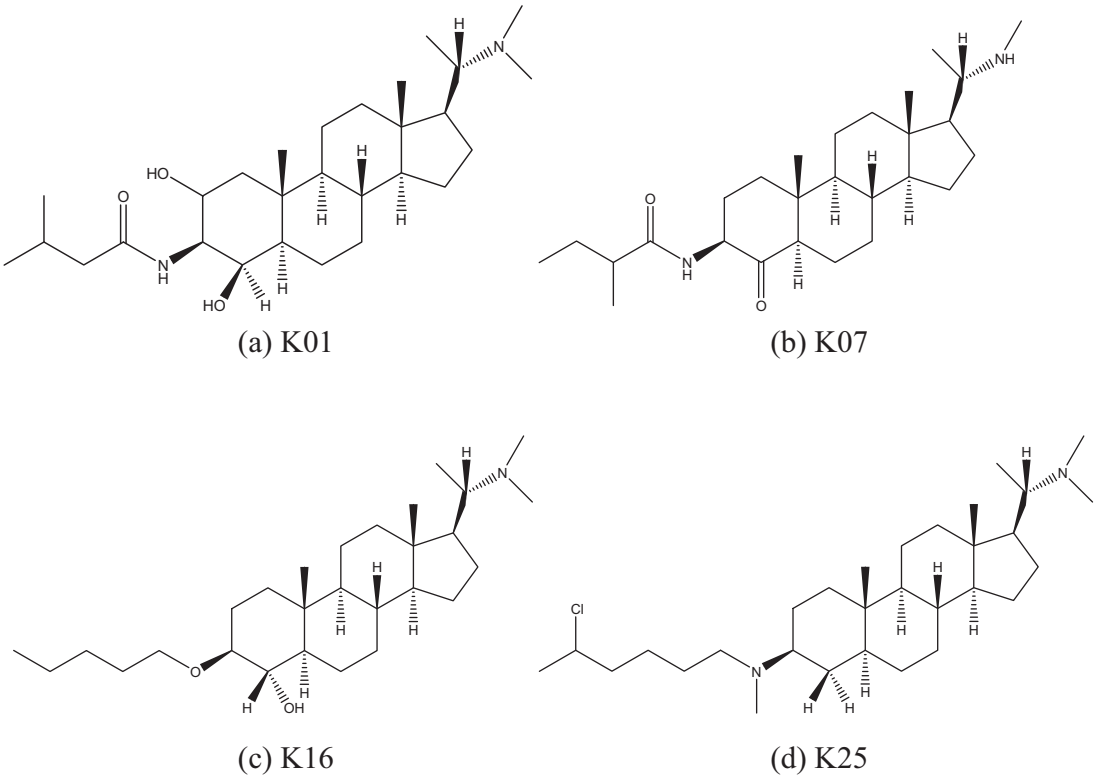

Fig. 1. Chemical structures of the ligand Kx employed in the present study; (a) K01, (b) K07, (c) K16 and (d) K25.

structure (PDB ID is 1P0P) [17], in order to confirm the adequacy of the docking procedure. The size of the grid box for docking was set as 15 × 15 × 15 Å, and the center of the box was set on the center of Trp82 of BChE, because the previous experiment [12] elucidated that Trp82 exists at the center of the active site of AChE and that BChE has a similar structure as AChE. The structure of BChE was fixed, and all dihedral angles of BCh were freely rotated in order to search for a variety of stable configurations for BCh docked to BChE. 200 candidate structures of the complex were created by using the genetic algorithm of Autodock 4.2, and they were classified into several clusters according to the value (2.0 Å) of the root mean square deviation (RMSD) between each of the structures created. It is noted that the atomic charges of BCh evaluated by the RESP (restrained electrostatic potential) [20] anaysis of Gaussian03 [15] based on HF/6-31G(d) were used in the docking, because the RESP charges can discribe the electrostatic interactions between BCh and the residues of BChE more accurately.

In the present study, the 200 candidate structures of BChE + BCh were classified into 22 clusters, and the cluster with the largest number of candidate structures was selected. Based on the docked-energy of Autodock 4.2, we picked up the most stable structure in the cluster as a candidate structure of BChE + BCh. To confirm the adequacy of this selection procedure, we compared the selected structure with that in the PDB structure [17]. The RMSD between them was evaluated to be 1.0 Å, indicating that the candidate structure of BChE + BCh created by the present docking procedure is comparable to the PDB structure. Therefore, in the present study, we created the candidate structures of the BChE + Kx complexes by the same docking procedure.

The candidate structures of the BChE + Kx complexes were fully optimized in water by the classical MM method. To consider the solvation effect on the complex properly, we added water molecules with an 8 Å layer around the complex and optimized the solvated structure by using AMBER12 [21], in which the AMBER99-SB [22] and TIP3P [23] force fields were assigned for the complex and the water molecules, respectively. The threshold value of the energy-gradient for the convergence in the optimization was set as 0.001 kcal/mol/Å. In the MM-optimizations, the atomic charges of each atom in the Kx ligands determined by the RESP analysis [20] were used for the AMBER99-SB force field.

2.2. FMO calculations of specific interactions between BChE and ligand

To elucidate the specific interactions and binding affinity between BChE and the Kx ligands, the electronic properties of the solvated BChE + Kx complexes optimized by the classical MM method were investigated by use of the *ab initio* FMO program ABINIT-MPX CREST [24], as the first step of the investigations for elucidating the specific interactions. It is noted that we should perform molecular dynamics (MD) simulations for searching the stable conformations of the solvated complexes more widely, and that the FMO calculation should be carried out for a number of structures obtained by the MD and MM-optimization, in order to obtain more realistic results considering the thermal fluctuation. However, these investigations are very time-consuming and impractical because of the large size of BChE. Therefore, we will try to perform them in the near future. In addition, it is impracticable to preform FMO calculations for the fully solvated structures, because the solvated structures of BChE + Kx have more than 3000 water molecules. We here considered the water molecules existing within a 5 Å distance from Kx explicitly and investigated electronic properties of BChE + Kx. In the FMO calculations, MP2 method was used to investigate accurately the π–π stacking, NH–π and CH–π interactions between the BChE residues and Kx, and the 6-31G basis-set was used.

The FMO method [25–33] has been developed for analyzing the electronic properties of large biomolecules such as proteins, DNA and RNA. In FMO calculations, a molecule is segmented into fragments, and based on the electronic properties evaluated for the monomers and the dimers of the fragments, the electronic properties of the whole molecule are evaluated. Since two cysteine residues in BChE form a disulfide bond, the two residues were assigned as a fragment. Each of the other residues of BChE, Kx, and each water molecule were assigned as a fragment, because this fragmentation enables us to evaluate the interaction energies between the amino acid residue, ligand, and solvating water molecules. From the inter fragment interaction energies (IFIE) [34] obtained by the FMO calculations, the important residues of BChE for the binding between BChE and Kx were highlighted at an electronic level.

In addition, we evaluated the total energies (TEs) for the solvated BChE + Kx structure, the solvated BChE, the solvated Kx and the solvating water molecules, in order to estimate the binding affinity between BChE and Kx. From these TEs, the binding energy (BE) between BChE and Kx was estimated from the following equation:

$$\mathrm{BE} = \mathrm{TE}(\mathrm{BChE} + \mathrm{Kx} + \mathrm{water}) - \mathrm{TE}(\mathrm{BChE} + \mathrm{water}) - \mathrm{TE}(\mathrm{Kx} + \mathrm{water}) + \mathrm{TE}(\mathrm{water}).$$

Here, TEs are total energies for each component of the solvated BChE + Kx complexes evaluated by the *ab initio* MP2/6-31G method of ABINIT-MPX CREST [24].

3. Results and discussion

3.1. Optimized structures of the solvated BChE + Kx complexes

The 200 candidate structures created by Autodock 4.2 [18] were classified into some clusters. Table 1 lists the number of structures in each cluster for the BChE + Kx complexes. The four types of ligands Kx were docked into almost the same position of the ligand-binding pocket of BChE with similar conformation, as shown in Fig. S2 of the supporting materials. This result is likely to come from the same framework structure of these Kx ligands. Table 1 indicates that about 10 clusters were created for the BChE + K16 and BChE + K25 complexes. Since K16 and K25 have a long $(CH_2)_n$ chain at the terminal position, as shown in Fig. 1c and d, these long chains cause a variety of conformations of K16 and K25 in the BChE + Kx complex. In fact, the chains of K16 and K25 stick out of the pocket, as shown in Fig. S2 of the supporting materials.

Table 1
Number of candidate structures in each cluster created by Autodock 4.2 [18] for BChE + Kx complexes.

Ranking of clusters	Number of structures			
	K01	K07	K16	K25
1	158	161	53	47
2	39	19	37	78
3	1	14	84	9
4	2	2	13	36
5	–	3	4	3
6	–	1	1	16
7	–	–	2	3
8	–	–	3	5
9	–	–	1	2
10	–	–	1	1
11	–	–	1	–

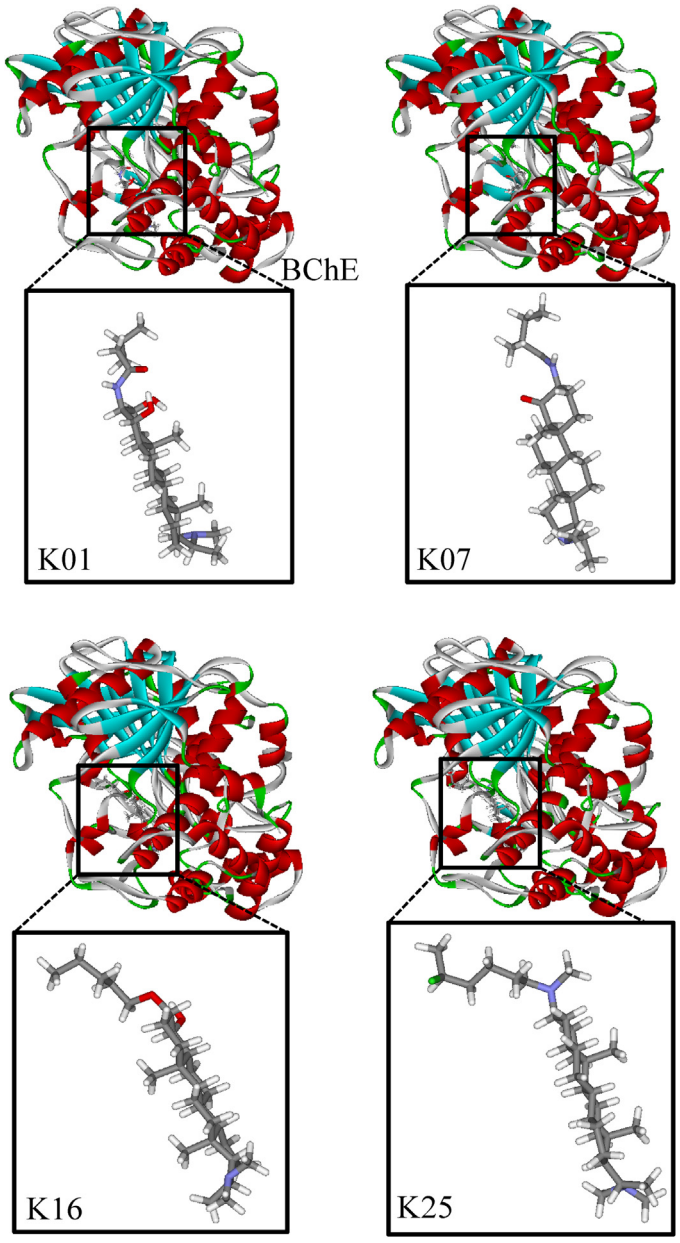

Fig. 2. Optimized structures for the BChE + Kx complexes in water, and conformations and structures of Kx in each optimized complex.

Among the clusters created by Autodock 4.2, we selected the cluster with the largest number of candidate structures, and based on the docked-energy of Autodock 4.2, we picked up the most stable structure in the cluster. The candidate structures of the BChE + Kx complexes were optimized by AMBER12 [21] in explicit water molecules. As shown in Fig. 2, all Kx ligands stabilize at the similar positions of the ligand-binding pocket of BChE, although the conformations and structures of Kx are significantly different to each other. Since the chemical structures of K01 and K07 are almost the same, their conformations in the BChE + Kx complex are similar as shown in Fig. 2. On the other hand, due to the long $(CH_2)_n$ chain of K16 and K25, their conformations are remarkably different from those for K01 and K07. In particular, K25 changes its structure to stabilize at the position, sticking out of the ligand-binding pocket of BChE.

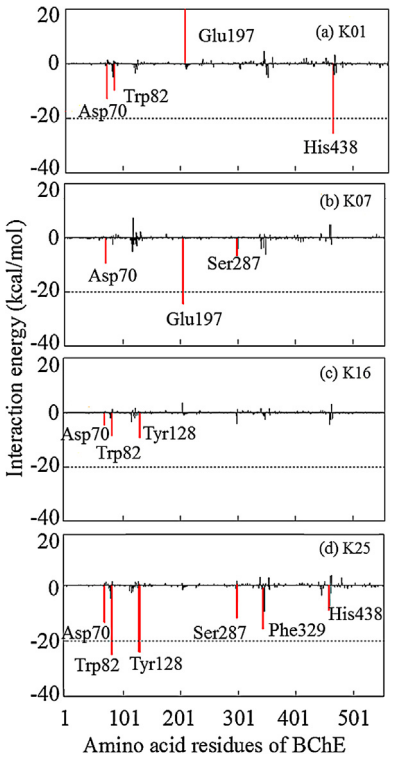

Fig. 3. Interaction energies between Kx and each amino acid residue of BChE evaluated by FMO.

3.2. Binding energy and specific interactions between BChE and Kx

The total energies (TEs) of the solvated BChE + Kx complex and the estimated binding energy (BE) between BChE and Kx are listed in Table 2, indicating that K25 has the greatest BE among the four ligands. To confirm the adequacy of the present molecular simulation, we analyzed the correlation between the BE evaluated and the IC_{50} obtained by our previous experiment [9]. As shown in Fig. S3 of the supporting materials, the correlation coefficient is 0.7, indicating that the size of BEs can describe the trend of IC_{50}. In principle, binding free energy (BFE) between BChE and Kx should be evaluated for predicting the binding affinity between BChE and Kx quantitatively. However, it is not practical to perform *ab initio* MO calculations for obtaining the free energies of the BChE + Kx complexes. It is expected from the present FMO results that the effect of entropy on BFE is almost the same for all the BChE + Kx complexes and that the trend of binding affinity between BChE and Kx can be estimated from the BE between BChE and Kx. Accordingly, in the present study, we proposed potent inhibitors to BChE, based on the BEs between BChE and Kx evaluated by the *ab initio* FMO method.

To elucidate which amino acid residues of BChE contribute to the binding between BChE and Kx, the interaction energies (IEs) between each residue of BChE and Kx were investigated by the MP2/6-31G method of ABINIT-MPX CREST [24]. Fig. 3 compares the results for K01, K07, K16 and K25. As for K25 having the greatest BE, Fig. 3d indicates that Trp82, Tyr128, Asp70, Ser287, Phe329 and His438 contribute to the binding between BChE and K25. There is no remarkable repulsive interaction between BChE and K25, resulting in the greater BE between BChE and K25. In contrast, K16 has the smallest BE and interacts weakly with Trp82, Tyr128 and Asp70. These weak attractive interactions are likely to cause the small BE between BChE and K16 shown in Table 2.

Table 2
Total energies (TE) of solvated BChE + Kx complexes and their component structures, and binding energies (BE) between BChE and Kx estimated from TEs, as BE = TE(BChE + Kx + water) − TE(BChE + water) − TE(Kx + water) + TE(water). The 50% inhibition concentration IC_{50} observed by the experiment [9] is listed for comparison.

	TE (kcal/mol)				BE (kcal/mol)	ΔBE (kcal/mol)	IC_{50} (μM)
	BChE + Kx + water	BChE + water	Kx + water	Water			
K01	−131,516,763.8	−130,622,244.2	−2,422,985.7	−1,528,518.3	−52.2	7.9	200.0
K07	−131,444,537.4	−130,622,280.1	−2,350,613.2	−1,528,408.6	−52.7	7.4	0.4
K16	−131,435,944.2	−130,622,289.7	−2,342,023.6	−1,528,418.2	−49.1	11.0	34.3
K25	−131,713,535.0	−130,622,292.1	−2,619,674.8	−1,528,492.0	−60.1	0.0	0.1
Proposed Kx							
K25-NH	−131,688,920.0	−130,622,196.0	−2,595,143.6	−1,528,480.1	−60.5	−0.4	–
K25-O	−131,759,833.0	−130,622,288.8	−2,665,948.7	−1,528,456.2	−51.7	8.4	–
K25-OH	−131,665,048.9	−130,526,764.4	−2,571,182.9	−1,432,950.6	−52.2	7.9	–

As shown in Fig. 3a and b, K01 and K07 have completely different interactions from those in the BChE + K16/K25 complexes. K01 has strong attractive interaction with His438, while it has strong repulsive interaction with Glu197. On the other hand, K07 has strong attractive interaction with Glu197, indicating that K01 and K07 have the opposite interactions with Glu197. As shown in Fig. 1, Kx have the same framework structure, so that it is difficult to predict the different specific interactions of Kx with

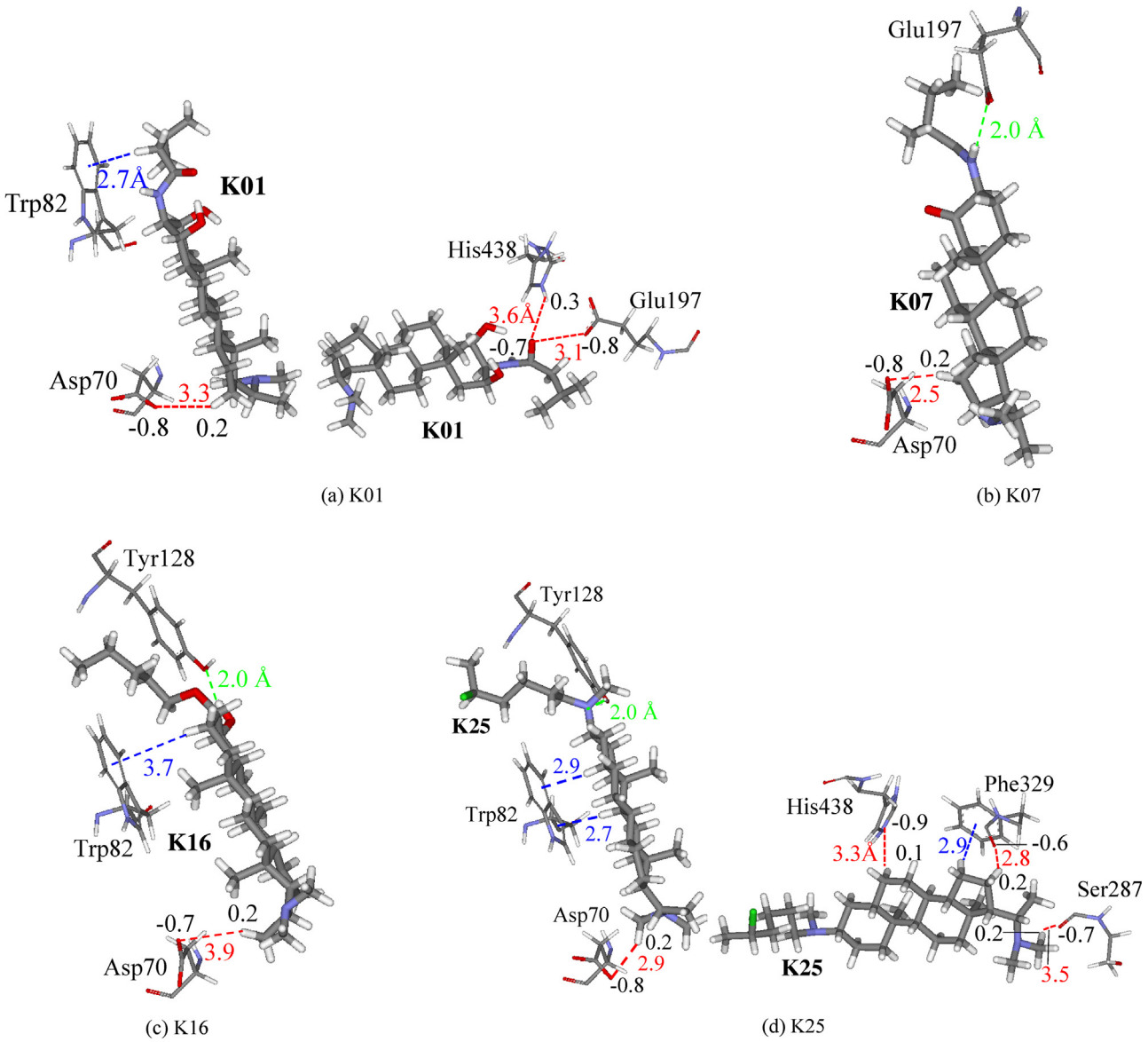

Fig. 4. Interacting structures between Kx and some residues of BChE; the red dashed lines indicate electrostatic interactions between charged atoms of BChE residues and Kx. The distances between atoms contributing to the interactions are shown in red, while the charges of the atoms are shown in black. The green dashed lines indicate hydrogen bonds, and the blue dashed lines indicate CH–π interactions (For interpretation of the references to color in this figure legend, the reader is referred to the web version of this article.)

BChE shown in Fig. 3 from only the difference in Kx structure. Our present FMO calculations for the MM-optimized structures of the solvated BChE + Kx complexes elucidate the significant difference in the specific interactions between BChE and Kx for the first time.

We furthermore investigated the structures around the Kx ligand in the BChE + Kx complexes, in order to elucidate the reason for the difference in specific interactions between BChE residues and Kx shown in Fig. 3. The structures are compared in Fig. 4, and the properties of each interaction are listed in Table S1 of the supporting materials.

As shown in Fig. 4d, the terminal methyl group of K25 interacts electrostatically at 2.9 Å with the oxygen atom of the Asp70 side-chain. In addition, two H atoms of the central hexagonal ring have CH–π interactions with the indole ring of Trp82 side-chain, and N atom of NMe group of K25 is hydrogen bonded with the OH group of Tyr128 side-chain. Due to these interactions, the residues Asp70, Trp82 and Tyr128 of BChE have strong attractive interactions to K25, resulting in the great BE between BChE and K25. In addition, the side-chains of Ser287, Phe329 and His438 interact with K25, as shown in Fig. 4d. Therefore, it is elucidated that K25 binds strongly with BChE by the above-mentioned interactions. It is thus expected that novel ligands based on K25 can be potent inhibitors to BChE.

The interactions between BChE and K16 are similar to those for K25, as shown in Fig. 4c. Since the distances between the BChE residues and K16 are longer that those for K25, the interactions between BChE and K16 are weaker, resulting in the smaller BE between BChE and K16.

Fig. 4a shows the interactions between the BChE residues and K01, in which the terminal methyl group of K01 interacts electrostatically at 3.3 Å with the oxygen atom of the Asp70 side-chain, in a similar way as K25. The indole ring of Trp82 contributes to the CH–π stacking interaction with the H atom of the $(CH_2)_n$ chain of K01. In addition, the C═O group of K01 and the terminal COO group of Glu197 exist at a short (3.1 Å) distance, leading to the strong repulsive interaction between K01 and Glu197, as shown in Fig. 3a. In addition, the C═O group interacts strongly with the His438 side-chain to cause the great attractive interaction between K01 and His438.

On the other hand, Fig. 4b indicates that the NH group of K07 and the COO group of Glu197 side-chain of BChE are hydrogen bonded to cause a strong attractive interaction between them, as shown in Fig. 3b. This interaction is never seen in the BChE + K01 complex, although K07 and K01 have almost the same chemical structure. Therefore, it is elucidated from the present FMO calculations that the small difference of structure between K01 and K07 causes the significant difference in the specific interactions between K01/K07 and Glu197 of BChE.

As mentioned above, small differences in structure of Kx ligands can cause the significant difference in the interactions between BChE and Kx. This fact cannot be elucidated by only comparing the structures of Kx and clarified only after performing the ligand-docking, MM-optimization and *ab initio* FMO calculations. In addition, the present FMO analysis elucidates that C═O group of K01, NH group of K07 and OH group of K16 are important for the attractive interactions between the BChE residues and these Kx ligands. Based on this result and K25, which has the greatest BE among the four Kx ligands, we created some novel ligands K25-NH, K25-O and K25-OH by introducing these important groups into K25. Their chemical structures are shown in Fig. 5, where the introduced group into K25 is indicated by a red dashed ellipse. The stable structures and electronic properties of BChE complexes with the novel Kx were investigated by the same way as for BChE + Kx, in order to propose novel potent inhibitors to BChE.

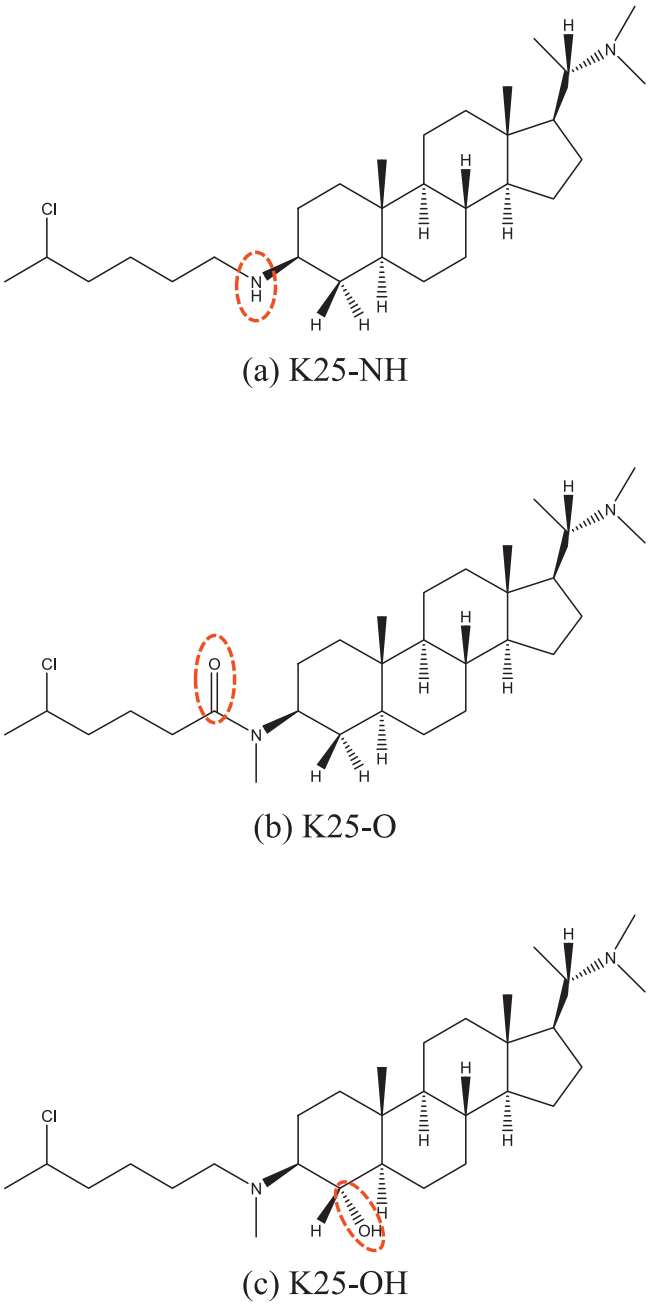

Fig. 5. Chemical structures of our proposed novel ligands based on K25. The introduced group into K25 is indicated by a red dashed ellipse.

3.3. *Binding energy and specific interactions between BChE and novel ligands*

Based on the BChE + K25 complex optimized by AMBER12 in water, the NH-, O- or OH-group was introduced into K25 as shown in Fig. 5 to make initial structures of BChE+K25-x, and they were fully optimized by AMBER12 in water. To elucidate the binding affinity of the novel K25-derivatives to BChE, the total energies (TEs) of the solvated complex and its component structures were evaluated for the optimized structures of the solvated complexes, and the BEs between BChE and K25-derivatives were estimated. As listed in the lower lines of Table 2, the BEs for K25-O and K25-OH are smaller than that for K25, indicating that the introduction of the O- and OH-group into K25 weakens the interaction between K25 and BChE. In contrast, the BE for K25-NH is a little (0.4 kcal/mol) greater

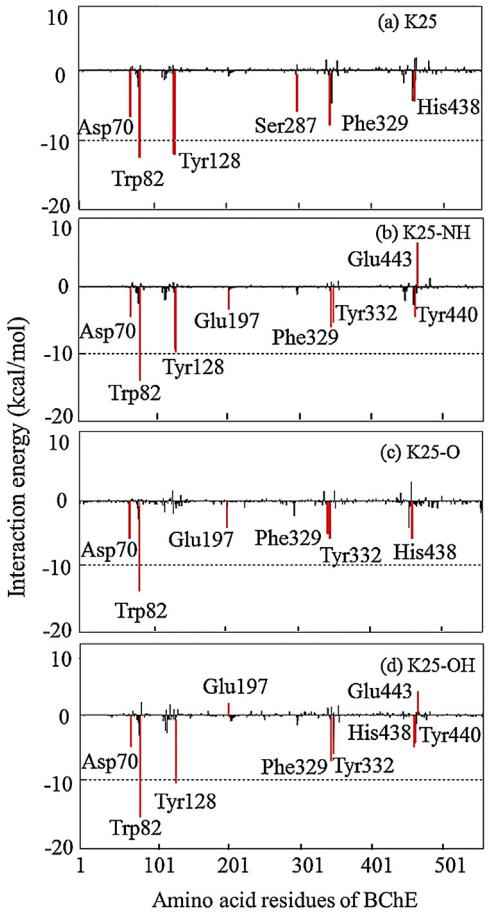

Fig. 6. Interaction energies between novel ligands and each amino acid residues of BChE evaluated by FMO.

than that for BChE + K25. Therefore, it is expected that K25-NH can be a potent ligand such as K25 for inhibiting the BChE function.

In order to elucidate the reason for the difference in BEs for these K25-derivatives, we investigated the interaction energies between the derivatives and each amino acid residue of BChE. From the comparison between Fig. 6a and b, it is elucidated that the interactions between K25 and Glu197, Tyr332 and Tyr440 are enlarged by introducing NH-group into K25. In contrast, the interactions between K25 and Asp70, Tyr128, Ser287 and His438 are weakened. In addition, K25-NH has strong repulsive interaction with Glu443. As a whole, the BE between BChE and K25 is a little enhanced by the introduction of NH-group. As shown in Fig. S4a of the supporting materials, K25-NH has a hydrogen bond with Glu197, while the hydrogen bond between K25 and Tyr128 is weakened by the NH-group. In addition, due to the effect of the NH-group introduction, the CH–π interactions between K25-NH and Phe329 and Tyr332 residues of BChE are produced, as indicated in Fig. S4a of the supporting materials. The specific interactions between K25 and Asp70 and Trp82 are not changed by the NH-group. These changes in structures around the K25 ligand induced by the NH introduction are consistent with the interaction energies shown in Fig. 6a and b.

As shown in Fig. 6c, K25-O has strong attractive interactions with Trp82, Asp70, Glu197, Phe329, Tyr332 and His438 of BChE. The remarkable change induced by the O-introduction into K25 is that the attractive interactions of K25 with Tyr128 and Ser287 are vanished by the introduction. This effect is likely to be a main reason for the reducing the BE between BChE and K25 by the O-introduction. In fact, the strong hydrogen bond between K25 and Tyr128 shown in Fig. 4d is not appeared in the complex of BChE + K25-O as shown in Fig. S4b.

K25-OH has attractive interactions with Trp82, Tyr128, Phe329, Tyr332, Asp70, His438 and Tyr440, as shown in Fig. 6d. This future is similar to that for K25. The OH introduction causes mainly the change in the interactions between K25 and Ser287, Tyr440 and Glu443, resulting in the reduction of BE between BChE and K25 by the OH introduction.

4. Conclusions

In order to propose potent inhibitors to BChE, we first conducted *ab initio* molecular simulations for the complexes of BChE with the existing inhibitors Kx investigated by the previous experiment [9]. From the results obtained by the *ab initio* FMO calculations, it was elucidated which Kx has strong binding affinity to BChE and which parts of the Kx contribute to the binding between Kx and BChE. Based on these simulated results, we proposed three types of novel compounds shown in Fig. 5 and investigated their specific binding properties to BChE. The results elucidate that K25-NH shown in Fig. 5a has a similar binding energy as the existing strong inhibitor K25. Therefore, it is expected that K25-NH can be a potent inhibitor to BChE.

Appendix A. Supplementary data

Supplementary data associated with this article can be found, in the online version, at http://dx.doi.org/10.1016/j.jmgm.2014.09.002.

References

[1] K.A. Phelan, M. Hollyday, Axon guidance in muscleless chick wings: the role of muscle cells in motoneuronal pathway selection and muscle nerve formation, J. Neurosci. 10 (1990) 2699–2716.
[2] R. Bischoff, Rapid adhesion of nerve cells to muscle fibers from adult rats is mediated by a sialic acid-binding receptor, J. Cell Biol. 102 (1986) 2273–2280.
[3] J. Arora, V. Kapur, R.K. Suri, R.Q. Khan, Inter-communications between median and musculocutaneous nerves with dual innervation of brachialis muscle – a case report, J. Anat. Soc. India 52 (2003) 66–68.
[4] C. Shelley, D.A. Jaco, L. Zhang, M. Marquez, D.B. Torre, P. Taylor, Acetylcholinesterase expression in muscle is specifically controlled by a promoter-selective enhance some in the first intron, J. Neurosci. 28 (2008) 2459–2470.
[5] Y. Dudai, M. Herzberg, I. Silman, Molecular structures of acetylcholinesterase from electric organ tissue of the electric eel, Proc. Natl. Acad. Sci. U. S. A. 70 (1973) 2473–2476.
[6] G. Lin, C.Y. Lai, W.C. Liao, P.S. Liao, C.H. Chan, Structure-reactivity relationships as probes to acetylcholinesterase inhibition mechanisms by aryl carbamates, J. Chin. Chem. Soc. 50 (2003) 1259–1265.
[7] A.N. Çokuğraş, Butyrylcholinesterase: structure and physiological importance, Turk. J. Biochem. 28 (2003) 54–61.
[8] H. Joachim, K. Cornelia, G.D. Ellen, L. Oksana, H.G. Nigel, K. Jochen, Excessive hippocampal acetylcholine levels in acetylcholinesterase-deficient mice are moderated by butyrylcholinesterase activity, J. Neurochem. 100 (2007) 1421–1429.
[9] M.T.K. Khan, Putative molecular interactions involving naturally occurring steroidal alkaloids from sarcococca hookeriana against acetyl- and butyrylcholinesterase, Curr. Bioinform. 8 (2013) 416–428.
[10] K.L. Davis, P. Powchik, Tacrine, Lancet 345 (1995) 625–630.
[11] M.W. Jann, Rivastigmine, a new-generation cholinesterase inhibitor for the treatment of Alzheimer's disease, Pharmacotherapy 20 (2000) 1–12.
[12] T. Okada, T. Murakawa, M.T.H. Khan, K. Komers, M. Kovářová, N. Kurita, Ab initio fragment molecular orbital calculations on specific interactions between acetylcholinesterase and its carbamate inhibitors, Curr. Top. Med. Chem. (2014) (in press).
[13] M. Kovářová, M.T.H. Khan, K. Komers, P. Pařík, A. Čegan, M. Zatloukalová, Kinetics of in vitro inhibition of acetylcholinesterase by nineteen new carbamates, Curr. Enzyme Inhib. 7 (2011) 236–243.
[14] B.J. Bennion, E.Y. Lau, J.-L. Fattebert, P. Huang, W. Corning, F.C. Lightstone, Modeling the binding of CWAs to AChE and BuChE, Mil. Med. Sci. Lett. 82 (2013) 1–13.
[15] M.J. Frisch, et al., Gaussian 03, Revision B. 04, Gaussian, Inc., Pittsburgh, PA, 2003.
[16] J. Wang, J. Gu, J. Leszczynski, Phosphonylation mechanisms of sarin and acetylcholinesterase: a model DFT study, J. Phys. Chem. B 110 (2006) 7567–7573.

[17] Y. Nicolet, O. Lockridge, P. Masson, J.C. Fontecilla-Camps, F. Nachon, Crystal structure of human butyrylcholinesterase and of its complexes with substrate and products, J. Biol. Chem. 278 (2003) 41141–41147.
[18] G.M. Morris, R. Huey, W. Lindstorm, M.F. Sanner, R.K. Belew, D.S. Goodsell, A.J. Olson, Autodock4 and AutodockTools4: automated docking with selective receptor flexibility, J. Comp. Chem. 16 (2009) 2785–2791.
[19] G.M. Morris, L.G. Green, Z. Radić, P. Taylor, K.B. Sharpless, A.J. Olson, F. Grynszpan, Automated docking with protein flexibility in the design of femtomolar "click chemistry" inhibitors of acetylcholinesterase, J. Chem. Inf. Model. 53 (2013) 898–906.
[20] B.H. Besler, K.M. Merz Jr., P.K. Kollman, Atomic charges derived from semiempirical methods, J. Comput. Chem. 11 (1990) 431–439.
[21] D.A. Case, et al., AMBER 12, University of California, San Francisco, 2012.
[22] W.D. Cornell, P. Cieplak, C.I. Bayly, I.R. Gould, K.M. Merz, D.M. Ferguson, D.C. Spellmeyer, T. Fox, J.W. Caldwell, P.A. Kollman, A second generation force field for the simulation of proteins, nucleic acids, and organic molecules, J. Am. Chem. Soc. 117 (1995) 5179–5197.
[23] L.J. William, C. Jayaraman, D.M. Jeffry, W.I. Roger, L.K. Michael, Comparison of simple potential functions for simulating liquid water, J. Chem. Phys. 79 (1983) 926–935.
[24] Y. Mochizuki, K. Yamashita, T. Murase, T. Nakano, K. Fukuzawa, K. Takematsu, H. Watanabe, S. Tanaka, Large scale FMO-MP2 calculations on a massively parallel-vector computer, Chem. Phys. Lett. 457 (2008) 396–403.
[25] D. Fedorov, K. Kitaura, Extending the power of quantum chemistry to large systems with the fragment molecular orbital method, J. Phys. Chem. A 111 (2007) 6904–6914.
[26] K. Kitaura, E. Ikeo, T. Asada, T. Nakano, M. Uebayasi, Fragment molecular orbital method: an approximate computational method for large molecules, Chem. Phys. Lett. 313 (1999) 701–706.
[27] K. Kitaura, T. Sawai, T. Asada, T. Nakano, M. Uebayasi, Pair interaction molecular orbital method: an approximate computational method for molecular interactions, Chem. Phys. Lett. 312 (1999) 319–324.
[28] T. Nakano, T. Kaminuma, T. Sato, Y. Akiyama, M. Uebayasi, K. Kitaura, Fragment molecular orbital method: application to polypeptides, Chem. Phys. Lett. 318 (2000) 614–618.
[29] T. Nakano, T. Kaminuma, T. Sato, K. Fukuzawa, Y. Akiyama, M. Uebayasi, K. Kitaura, Fragment molecular orbital method: use of approximate electrostatic potential, Chem. Phys. Lett. 351 (2002) 475–480.
[30] K. Kitaura, S. Sugiki, T. Nakano, Y. Komeiji, M. Uebayasi, Fragment molecular orbital method: analytical energy gradients, Chem. Phys. Lett. 336 (2001) 163–170.
[31] M. Ito, K. Fukuzawa, T. Ishikawa, Y. Mochizuki, T. Nakano, S. Tanaka, Ab initio fragment molecular orbital study of molecular interactions in liganded retinoid X receptor: specification of residues associated with ligand inducible information transmission, J. Phys. Chem. B 112 (2008) 12081–12094.
[32] Y. Mochizuki, K. Yamashita, T. Murase, T. Nakano, K. Fukuzawa, K. Takematsu, H. Watanabe, S. Tanaka, Large scale FMO-MP2 calculations on a massively parallel vector computer, Chem. Phys. Lett. 457 (2008) 396–403.
[33] D.G. Fedorov, T. Nagata, K. Kitaura, Exploring chemistry with the fragment molecular orbital method, Phys. Chem. Chem. Phys. 14 (2012) 7562–7577.
[34] K. Fukuzawa, T. Nakano, A. Kato, Y. Mochizuki, S. Tanaka, Applications of the fragment molecular orbital method for bio-macromolecules, J. Comput. Chem. 6 (2007) 185–198.